Chinese Physical Society | IOP Publishing
CPB
Chinese Physics B
http://cpb.iphy.ac.cn https://iopscience.iop.org/journal/1674-1056

Enhanced timing of a 113 km O-TWTFT link with complex maximum likelihood estimation process

Yu-Chen Fang(方宇辰), Jian-Yu Guan(管建宇), Qi Shen(沈奇), Jin-Jian Han(韩金剑), Lei Hou(侯磊), Meng-Zhe Lian(连蒙浙), Yong Wang(王勇), Wei-Yue Liu(刘蔚悦), Ji-Gang Ren(任继刚), Cheng-Zhi Peng(彭承志), Qiang Zhang(张强), Hai-Feng Jiang(姜海峰), and Jian-Wei Pan(潘建伟)

Citation: Chin. Phys. B, 2026, 35 (**1**): 010602. DOI: 10.1088/1674-1056/ae1120
http://cpb.iphy.ac.cn; http://iopscience.iop.org/cpb

What follows is a list of articles you may be interested in

Finite time hybrid synchronization of heterogeneous duplex complex networks via time-varying intermittent control

Cheng-Jun Xie(解成俊) and Xiang-Qing Lu(卢向清)
Chin. Phys. B, 2025, 34 (**4**): 040601. DOI: 10.1088/1674-1056/adacc6

A real-time performance improvement method for composite time scale

Fangmin Wang(王芳敏), Wenlin Li(李汶林), Hongfei Dai(戴鸿飞), Chunyi Li(李春怡), Jianhua Zhou(周建华), Shenhui Xue(薛申辉), and Bo Wang(王波)
Chin. Phys. B, 2024, 33 (**9**): 090601. DOI: 10.1088/1674-1056/ad6131

A 532 nm molecular iodine optical frequency standard based on modulation transfer spectroscopy

Feihu Cheng(程飞虎), Ning Jin(金宁), Fenglei Zhang(张风雷), Hui Li(李慧), Yuanbo Du(杜远博), Jie Zhang(张洁), Ke Deng(邓科), and Zehuang Lu(陆泽晃)
Chin. Phys. B, 2021, 30 (**5**): 050603. DOI: 10.1088/1674-1056/abd754

An Yb-fiber frequency comb phase-locked to microwave standard and optical reference

Hui-Bo Wang(汪会波), Hai-Nian Han(韩海年), Zi-Yue Zhang(张子越), Xiao-Dong Shao(邵晓东), Jiang-Feng Zhu(朱江峰), Zhi-Yi Wei(魏志义)
Chin. Phys. B, 2020, 29 (**3**): 030601. DOI: 10.1088/1674-1056/ab696d

Photonic generation of RF and microwave signal with relative frequency instability of 10^{-15}

Lu-Lu Yan(闫露露), Wen-Yu Zhao(赵文宇), Yan-Yan Zhang(张颜艳), Zhao-Yang Tai(邰朝阳), Pan Zhang(张攀), Bing-Jie Rao(饶冰洁), Kai Ning(宁凯), Xiao-Fei Zhang(张晓斐), Wen-Ge Guo(郭文阁), Shou-Gang Zhang(张首刚), Hai-Feng Jiang(姜海峰)
Chin. Phys. B, 2018, 27 (**3**): 030601. DOI: 10.1088/1674-1056/27/3/030601

RAPID COMMUNICATION

Enhanced timing of a 113 km O-TWTFT link with complex maximum likelihood estimation process

Yu-Chen Fang(方宇辰)[1,2,3,†], Jian-Yu Guan(管建宇)[2,3,†], Qi Shen(沈奇)[1,2,3], Jin-Jian Han(韩金剑)[1,2,3], Lei Hou(侯磊)[2,3] Meng-Zhe Lian(连蒙浙)[1,2,3], Yong Wang(王勇)[4], Wei-Yue Liu(刘蔚悦)[2,3,5], Ji-Gang Ren(任继刚)[1,2,3], Cheng-Zhi Peng(彭承志)[1,2,3], Qiang Zhang(张强)[1,2,3], Hai-Feng Jiang(姜海峰)[1,2,3,‡], and Jian-Wei Pan(潘建伟)[1,2,3]

[1] *Hefei National Research Center for Physical Sciences at the Microscale and School of Physical Sciences, University of Science and Technology of China, Hefei* 230026, *China*

[2] *Shanghai Research Center for Quantum Sciences and CAS Center for Excellence in Quantum Information and Quantum Physics, University of Science and Technology of China, Shanghai* 201315, *China*

[3] *Hefei National Laboratory, University of Science and Technology of China, Hefei* 230088, *China*

[4] *Xinjiang Astronomical Observatory, Chinese Academy of Sciences, Urumqi* 830011, *China*

[5] *Faculty of Information Science and Engineering, Ningbo University, Ningbo* 315211, *China*

(Received 10 September 2025; revised manuscript received 25 September 2025; accepted manuscript online 9 October 2025)

Optical two-way time-frequency transfer (O-TWTFT), utilizing optical frequency comb carriers and linear optical sampling, effectively enables space-to-ground optical frequency standard comparisons. Previously reported detection sensitivities of O-TWTFTs were typically in the nanoWatt level, necessitating high-power optical frequency combs to compensate for significant losses in high-orbit satellite-to-ground passes. Such hardware-based solutions, while effective, tend to be costly. This paper presents a novel data post-processing algorithm to enhance sensitivity. Unlike previous timing methods, which depend solely on optical phase data and discard intensity information — resulting in elevated errors, especially under low-reception power, our approach employs complex least squares (CLS) estimation in the complex frequency domain. By preserving all intermediate data and avoiding noise from phase unwrapping, it achieves superior sensitivity and accuracy. Experiments over a 113-kilometer free-space link validate the algorithm's robustness, delivering a detection sensitivity of 0.1 nanoWatts — over tenfold better than prior techniques — despite a 100-decibel link loss, comparable to Earth–Moon optical links.

Keywords: optical time-frequency transfer, linear optical sampling, frequency comb, complex least squares

PACS: 06.30.Ft, 42.62.Eh, 42.79.Sz

DOI: 10.1088/1674-1056/ae1120 **CSTR:** 32038.14.CPB.ae1120

1. Introduction

The advancement of optical clocks has necessitated the development of high-precision time and frequency transfer systems on a global scale. State-of-the-art optical clocks have achieved remarkable instability and uncertainty levels of 10^{-19},[1–5] surpassing the best primary frequency standards by over an order of magnitude. These precision levels are essential for applications such as the redefinition of the second[6] and precision geodesy.[7,8] While fiber-based links can meet these demands, their global deployment is hindered by cost and complexity in the near future.

Current global time and frequency transfer relies on satellite-based relays. But none meets the requirement of optical clock frequency transfer. Ground-satellite links require a large unambiguous timing range for continuous operation due to the noisy and unstable atmospheric conditions. Traditional microwave signals, used as carriers, limit long-term instability to a few picoseconds due to their low timing resolution. Time transfer by laser link (T2L2), which uses pulse lasers and photodetectors, faces similar limitations.[9,10]

The most viable solution is the optical two-way time-frequency transfer (O-TWTFT), which employs the two-way transmission of coherent pulse laser trains, i.e., optical frequency combs (OFCs), combined with linear optical sampling (LOS).[11] The LOS method involves interfering a local OFC with a received OFC of a slightly different repetition rate, allowing the local comb's pulses to continuously traverse the signal pulse. The OFC's nanosecond-level pulse interval provides a large unambiguous timing range, facilitating link reconnection after interruptions.

Achieving a ground-satellite O-TWTFT link requires overcoming transmission losses ranging from tens to over a hundred dB, depending on the distance and optical transceiver's effective aperture. In 2022, we demonstrated an

†These authors contributed equally to this work.

‡Corresponding author. E-mail: hjiang1@ustc.edu.cn

89-dB, 113-km O-TWTFT link with an instability of 10^{-19} at 10000 s, using an OFC power of up to 1 W and detection sensitivity in the nanoWatt range.[12] This high tolerance for loss is suitable for GEO/IGSO satellite-to-ground links but falls short for deep space applications like Moon–Earth links.

An alternative method to improve loss tolerance is optical frequency comb tracking,[13,14] which modulates the local comb to interfere synchronously with the received signal, enhancing optical signal utilization. Static link experiments demonstrate sub-picoWatt timing sensitivity; however, this approach requires complex, fast-tracking hardware to manage significant Doppler shifts, and experimental realization under such dynamic conditions has not yet been achieved.[14]

This study builds on the proven O-TWTFT technology, validated for diverse scenarios, including Doppler effects and multi-node setups. Previous time extraction involves: (1) applying a fast Fourier transform to convert time-domain signals into complex frequency-domain spectra; (2) extracting phase data with phase unwrapping to correct periodic phase transitions; and (3) estimating time via least squares from the frequency–phase relationship. We found that discarding amplitude in step two increases time estimation errors, while phase unwrapping introduces significant inaccuracies under low-power conditions. Our innovation eliminates phase unwrapping by directly using complex frequency-domain data for time fitting, improving detection sensitivity and accuracy without hardware changes. This approach, though computationally intensive due to multi-parameter fitting, offers a robust software-based solution.

2. Time extraction algorithm

O-TWTFT derives clock offsets by differentiating two one-way delay measurements, a method predicated on the assumption of noise process symmetry in both links. Crucially, the performance enhancement of O-TWTFT depends on achieving high-precision one-way delay measurements, which can be achieved using linear optical sampling (LOS). As shown in Fig. 1(a), LOS consists of two frequency combs — a local comb operating at a repetition frequency f_r and an incoming comb with a deviation of Δf_r. The electric fields of the two combs can be written as

$$E_{\text{local}}(t) = \mathrm{e}^{\mathrm{i}2\pi\nu_l t}\sum_{n=0}^{N} E_{l,n}\,\mathrm{e}^{\mathrm{i}2\pi n f_r t}, \tag{1}$$

$$E_{\text{sig}}(t) = \mathrm{e}^{\mathrm{i}2\pi\nu_s(t-\tau)}\sum_{n=0}^{N} E_{s,n}\,\mathrm{e}^{\mathrm{i}2\pi n(f_r+\Delta f_r)(t-\tau)}. \tag{2}$$

Here, ν_l and ν_s are carrier frequencies of local and signal combs, $E_{l,n}$ and $E_{s,n}$ denote the spectrum intensity distributions of local and signal combs, and τ denotes the one-way delay. The two combs interfere and generate a series of voltage data at the detector with a proper low-pass filter (see supplementary of Ref. [11]):

$$\begin{aligned} V(t) &\propto \mathrm{Im}[E^*_{\text{local}}(t)E_{\text{sig}}(t)] \\ &= \mathrm{Im}[\mathrm{e}^{-\mathrm{i}2\pi\nu_s\tau}\,\mathrm{e}^{\mathrm{i}2\pi(\nu_s-\nu_l)t} \\ &\quad \times \sum_{n=0}^{N} E_{l,n}E_{s,n}\,\mathrm{e}^{-\mathrm{i}2\pi n(f_r+\Delta f_r)\tau}\,\mathrm{e}^{\mathrm{i}2\pi n\Delta f_r t}], \end{aligned} \tag{3}$$

which is a periodic centerburst signal in the time domain. Each centerburst signal represents a single measurement and we call it an interferogram.

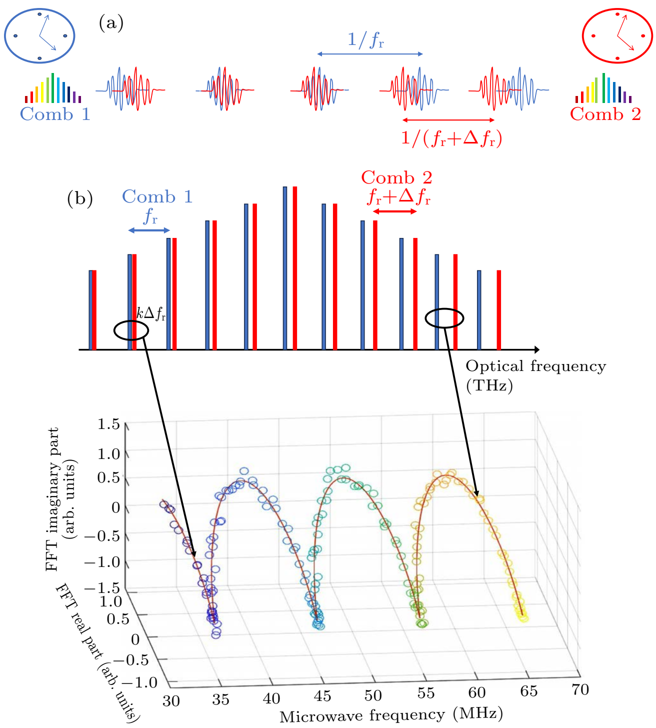

Fig. 1. (a) The time domain picture of O-TWTFT. The two terminals exchange frequency comb pulse trains, where their repetition rates, denoted as f_{r1} and f_{r2}, are offset by a small frequency difference Δf_r. (b) The upper part of the figure presents a schematic that illustrates the optical spectra of comb 1 (in blue) and comb 2 (in red). The interference of the two combs creates a series of beat frequencies after a proper filter. The lower part of the figure depicts the CLS algorithm schematic. After the interferogram undergoes Fourier transformation and is divided by the corresponding points of the Fourier transformation of the reference interferogram, the resulting pattern theoretically forms a spiral line (parameterized by $\beta\,\mathrm{e}^{\mathrm{i}(k\alpha+\gamma)}$) within the space composed of the complex plane and the frequency axis (k).

For conventional LOS, one first performs a fast Fourier transform (FFT) on the interferogram data, yielding a complex spectrum $S(f)$. After calculating the phase difference $\Delta\angle S(f)$ relative to a reference interferogram (with delay τ_{ref}), the residual phase is proportional to the change in delay $\Delta\tau = \tau - \tau_{\text{ref}}$ and the FFT frequency f:

$$\Delta\angle S(f) = -2\pi\nu_s\Delta\tau - 2\pi\frac{f-(\nu_s-\nu_l)}{\Delta f_r}(f_r+\Delta f_r)\Delta\tau. \tag{4}$$

The change in one-way delay $\Delta\tau$ can be solved from the slope of $\Delta\angle S(f)$ versus f. The main obstacle in conventional LOS is that the phase $\Delta\angle S(f)$ is wrapped. Reliable one-dimensional phase unwrapping[15,16] becomes extremely challenging at low signal-to-noise ratios (SNR), and even algorithms optimized for O-TWTFT[17] struggle, introducing errors and limiting detection sensitivity.

Previous methods[12] utilize only the phase information from the FFT, requiring unwrapping and least-squares fitting of the phase slope to estimate time delay. In contrast, we propose the complex least squares (CLS) method, which directly employs the full complex FFT data (amplitude and phase), avoiding phase unwrapping entirely (as illustrated in Fig. 1(b)).

The CLS algorithm is introduced as follows. We will denote the complex FFT values within the effective spectrum of the reference interferogram as A_k, and those for the current interferogram as C_k, where k is the frequency bin index. Inspired by Eq. (4), which shows that the spectral phase difference is linear with frequency, we construct a model to predict the current spectrum (B_k) from the reference spectrum (A_k):

$$B_k = A_k \cdot \beta\, \mathrm{e}^{\mathrm{i}(k\alpha+\gamma)}. \tag{5}$$

Here, β represents the relative amplitude change, and the phase term $k\alpha+\gamma$ models the linear phase difference. The parameter γ is a constant phase offset, and α is the slope of the phase difference versus the frequency bin index k. Crucially, α is directly proportional to the change in one-way time delay $\Delta\tau$:

$$\Delta\tau = -\alpha \cdot \frac{\Delta f_{\mathrm{r}}}{2\pi\delta f(f_{\mathrm{r}}+\Delta f_{\mathrm{r}})}, \tag{6}$$

where δf is the frequency spacing per bin. It is this delay variation, $\Delta\tau$, that represents the timing signal to be measured and constitutes the final output of our algorithm for each interferogram.

Our goal is to find the optimal values of α, β, γ to minimize the loss function, defined as the sum of squared complex errors $e_k = B_k - C_k$:

$$\mathrm{loss} = \sum_k |e_k|^2 = \sum_k |A_k\beta\, \mathrm{e}^{\mathrm{i}(k\alpha+\gamma)} - C_k|^2. \tag{7}$$

Minimizing this loss function (Eq. (7)) is equivalent to a maximum likelihood estimation (MLE) of the parameters (α,β,γ), under the assumption that the noise ($C_k - B_k$) is complex additive white Gaussian noise (AWGN). This assumption is reasonable for detector and shot noise dominating single-interferogram measurements (justification provided in the supplementary material).

The CLS method offers the following key advantages over traditional phase-only fitting. (1) It completely bypasses the problematic phase unwrapping step, thus avoiding the unwrapping errors that plague low-SNR measurements. (2) It utilizes the full complex information (both amplitude and phase) from the Fourier spectrum, whereas conventional methods discard the amplitude. In a functional sense, the amplitude information serves as a weighting factor, which effectively reduces the error variance. Although computationally more demanding, CLS significantly enhances the robustness and precision of time extraction, especially at ultra-low SNR. A detailed explanation and further elaboration of this algorithm are provided in the supplementary material.

3. Experimental setup

To rigorously evaluate the performance of our proposed CLS algorithm, especially under low-SNR scenarios, we conducted time-frequency transfer experiments in Ürümqi, Xinjiang, with received power as low as 0.1 nW. The experimental setup essentially replicated that reported in Ref. [12], except for an optical attenuator inserted into the link to introduce additional loss. At such ultralow power levels, interferogram signals suffered complete submergence in noise, rendering the original level-triggered acquisition scheme ineffective. Consequently, we implemented quasi-continuous data sampling under low received power, followed by a proper postprocessing method with the CLS algorithm. The detailed steps for data filtering can be found in Section II of supplementary material. The detailed setup is shown in Fig. 2. Two terminals, situated in Nanshan and Gaoyazi, are 113 km apart and are equipped with an ultra-stable laser (USL), two high-power OFCs, two LOS modules, two computational modules, and optical transceiver telescopes. By employing frequency multiplexing within a shared free-space channel, we established two independent two-way time-frequency transfer links. We intentionally increased the loss on the 1545-nm link to generate a dataset for algorithm comparison, using the 1563-nm link with lower loss as a control.

Each terminal houses a USL with a frequency instability of 3×10^{-15} at 1 second and a wavelength (λ) of 1550.12 nm, serving as the reference clock source. The OFCs, optically phase-locked to the USL, function as carrier and reference signals. The 1545-nm OFC operates at a 250 MHz repetition rate with a 2.5 kHz differential repetition rate between terminals, while the 1563-nm OFC has a 200 MHz repetition rate with a 2 kHz differential rate. To counteract the significant link loss, we utilized a two-stage high-power erbium-doped fiber amplifier (EDFA), achieving a 1-W output power with a 20-nm filtered spectrum. The 3-dB bandwidth of the OFCs at both wavelengths was restricted to approximately 7 nm by the gain region of the EDFA. In the LOS modules, interference data is detected by a balanced photodetector, and low-pass filtered (bandwidth $\sim$ 100 MHz) to isolate only a single copy of the baseband interferogram spectrum for subsequent processing. This differs from approaches that might average multiple spectral copies.[18] The data is then digitized, and sent to the calculation module for processing. The optical transceiver telescopes, with automatic direction tracking, use an orthogonal polarization scheme to differentiate between sending and receiving OFCs, providing substantial isolation in two-way transfer and mimicking a satellite-to-ground scenario with relative angular motion distinguishing backward and forward transfers.

The 1563-nm link demonstrates an average link loss of approximately 75 dB. The performance at such loss has been validated in previous experiments,[12] so the previous algorithm's result on the 1563-nm link serves as the gold-standard reference due to its established validity. In contrast, the 1545-nm link experiences a significantly higher average link loss, estimated at 90 dB. By applying both the previous algorithm and the CLS algorithm on the 1545-nm link while referencing their outcomes against the 1563-nm benchmark, we quantitatively evaluate the performance of these algorithms.

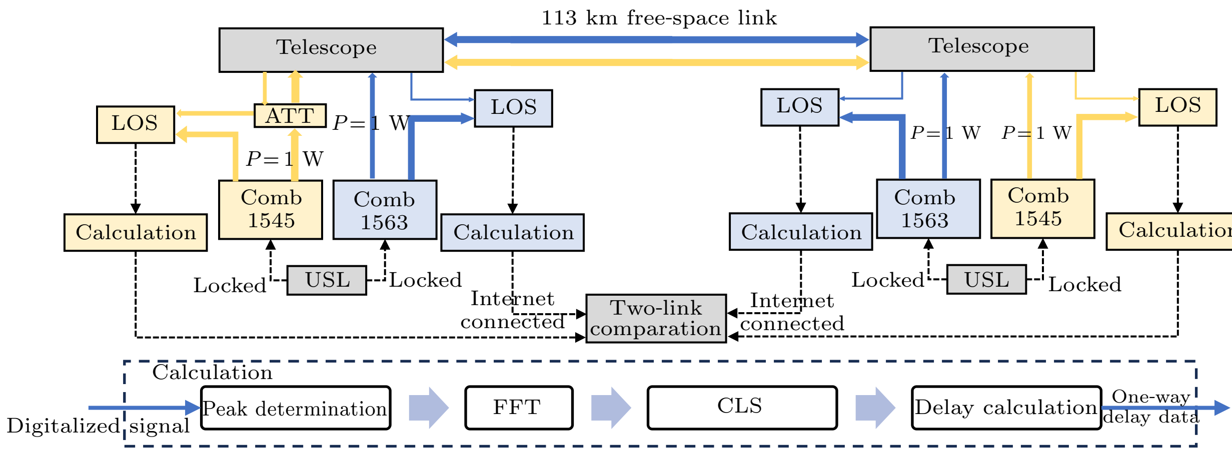

Fig. 2. Experimental setup. The schematic illustrates two free-space links, with the 1545-nm link in yellow and the 1563-nm link in blue. The lower section details the computational steps within the computation module, including the phase unwrapping process performed using both the CLS algorithm and the previous algorithm[17] for comparison.

4. Results

Figure 3(a) presents the time deviation (TDEV) for both the CLS and previous algorithms. The average received power for the valid data utilized by the CLS algorithm was 2.2 nW, compared to 3.8 nW for the previous algorithm, reflecting the CLS algorithm's enhanced sensitivity. Over short averaging intervals ($\tau < 100$ s), the TDEV of both algorithms exhibits a downward trend, with the slope being proportional to $\tau^{-1/2}$, characteristic of white phase noise limited performance. Notably, the CLS algorithm demonstrates superior stability compared to the previous algorithm at each averaging point. The CLS algorithm's TDEV starts at 50 fs and improves to 1 fs within approximately 100 seconds, whereas the previous algorithm begins at a higher TDEV of 80 fs. The CLS algorithm also collects more valid data, with an average data rate of 280 samples per second, compared to 130 samples per second for the previous algorithm, which struggles with processing interferograms with a received power less than 1 nW. For averaging periods less than 100 seconds, the previous algorithm fails to match the performance of the CLS algorithm. At longer averaging times ($\tau > 100$ s), the TDEV curves tend to converge because of system drift domination. This drift is primarily attributed to temperature fluctuations affecting a short section of uncompensated optical fiber within the setup, and we observed a correlation between the TDEV bump and the laboratory's air conditioning cycle. This is beyond the scope of the CLS algorithms. To explore the performance limits of the CLS algorithm, we also present the TDEV curve calculated only from data points with received power around 0.1 nW (filtered from the full dataset). Due to atmospheric turbulence, the instantaneous received power fluctuates significantly. The 0.1 nW represents the instantaneous power calculated directly from the signal amplitude of specific interferograms (see supplementary material). This indicates that even at the much lower data rates associated with this minimum power level, the CLS algorithm's TDEV can reach below sub-femtoseconds at 10000 seconds of averaging. Details on selecting specific received power and filtering valid data can be found in the supplementary material.

Figure 3(b) illustrates the standard deviation as a function of received optical power for the high-loss 1545-nm link, for both algorithms. As signal power decreases, the SNR of the interferograms diminishes, leading to an increase in the standard deviation of the results. The CLS algorithm's curve is consistently lower than that of the previous algorithm, indicating its effectiveness in reducing estimation errors under low SNR conditions. The superior performance of CLS, both in TDEV (Fig. 3(a) at short τ) and single-shot precision (Fig. 3(b)), stems from key advantages discussed in Section 2 and supplementary material. First, as an MLE process, CLS optimally utilizes the full complex information (amplitude and phase) across the entire effective spectrum, acting akin to a matched filter. In contrast, the previous phase-only method discards amplitude information and, critically, suffers from phase-unwrapping 'cycle-slip' errors at low SNR, introducing significant technical noise far above the fundamental limit.[17] Second, by avoiding phase unwrapping entirely, CLS is inherently more robust at very low SNR. This enhanced per-measurement precision directly translates to the improved short-term TDEV shown in Fig. 3(a). In extremely low SNR scenarios, both algorithms may produce erroneous results that deviate significantly from the true value. We define the minimum received power for an algorithm as the threshold at which 99% of its output data falls within three standard deviations (after filtering, see supplementary material). The CLS algorithm's minimum received power is approximately 0.1 nW, an order-of-magnitude improvement compared to the previous algorithm's limit of about 1 nW. Figure 3(b) also displays the fundamental shot-noise limit inherent to the LOS technique for a single interferogram measurement:[21,22]

$$\sigma_{\mathrm{t}}^2 \approx \frac{\tau_{\mathrm{p}}^2}{\mathrm{SNR}}, \tag{8}$$

where τ_{p} represents the intensity full width half maximum (FWHM) of the unchirped frequency comb pulses, and $\mathrm{SNR} \approx \frac{3\eta M \tau_{\mathrm{p}} P_{\mathrm{rec}}}{h\nu}$ is the shot-noise-limited signal-to-noise ratio of a single, baseband interferogram, as shown in Eq. (A5) of Ref. [21]. This SNR gap compared to conventional shot-noise-limited interferometric SNR arises because the LOS scheme employs two optical frequency combs with slightly different repetition rates. Therefore, in fact, only the pairs of laser pulses that are simultaneously arriving contribute to the interference signal. Our results demonstrate that under low received power conditions, the CLS algorithm's precision approaches the LOS shot-noise limit defined by the equation.

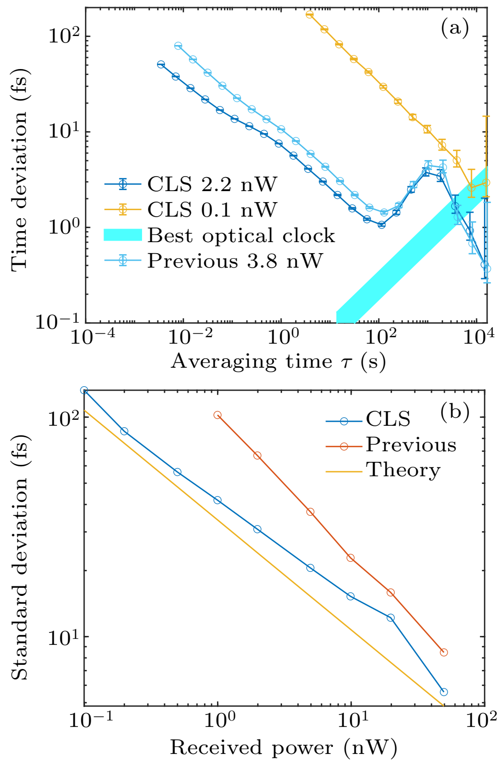

Fig. 3. (a) Time deviation (TDEV) comparison for the 1545-nm link. The CLS algorithm outperforms the previous algorithm by half an order of magnitude at short averaging times. The average received power among valid data for the previous algorithm is 3.8 nW, while for the CLS algorithm, it is 2.2 nW, reflecting their respective minimum received power capabilities. The TDEV curve for the CLS algorithm at 0.1-nW filtered data (data points around 0.1 nW selected from the full dataset) parallels the other curves over long integration times, indicating negligible long-term stability impact under such a low signal power. Performances of top optical clocks are also shown for comparison.[19,20] (b) The relationship between the single-shot measurement standard deviation and received power for the 1545-nm link, with the blue line for the CLS algorithm and the orange line for the previous algorithm. The collected data in one round of the experiment is binned by received power. The standard deviation of each bin is then calculated. The CLS algorithm's performance approaches the shot-noise limit for the LOS technique, represented by the yellow line.

5. Conclusion

We proposed and experimentally validated the application of the complex least squares (CLS) algorithm for time extraction in O-TWTFT, which enhances the system's detection sensitivity and timing accuracy. Previous timing algorithms relied exclusively on fitting the unwrapped spectral phase, leading to significant timing errors under low signal-to-noise ratio (SNR) conditions. In contrast, the CLS method fully exploits the complex information of the interferogram spectrum (both amplitude and phase), additionally avoiding the error-prone phase unwrapping step. Experimental results demonstrate that the minimum received power requirement has been reduced by an order of magnitude, from 1 nW to 0.1 nW. Additionally, the short-term time standard deviation has decreased from 80 fs to 50 fs. For O-TWTFT systems equipped with Watt-level optical frequency combs (OFCs), the CLS algorithm enables the total system loss to reach 100 dB, equivalent to the Earth–Moon link loss.

Acknowledgements

This research was supported by the National Key Research and Development Programme of China (Grant Nos. 2020YFC2200103 and 2020YFA0309800), the National Natural Science Foundation of China (Grant No. T2125010), Strategic Priority Research Programme of Chinese Academy of Sciences (Grant No. XDB35030000), Anhui Initiative in Quantum Information Technologies (Grant No. AHY010100), Key R&D Plan of Shandong Province (Grant No. 2021ZDPT01), Shanghai Municipal Science and Technology Major Project (Grant No. 2019SHZDZX01), and Innovation Programme for Quantum Science and Technology (Grant Nos. 2021ZD0300100, 2021ZD0300300, and 2021ZD0300903).

References

[1] Brewer S M, Chen J S, Hankin A M, Clements E R, Chou C W, Wineland D J, Hume D B and Leibrandt D R 2019 *Phys. Rev. Lett.* **123** 033201
[2] Bothwell T, Kedar D, Oelker E, Robinson J M, Bromley S L, Tew W L, Ye J and Kennedy C J 2019 *Metrologia* **56** 065004
[3] Nicholson T L, Campbell S, Hutson R, Marti G E, Bloom B, McNally R L, Zhang W, Barrett M, Safronova M S, Strouse G, *et al.* 2015 *Nat. Commun.* **6** 6896

[4] Huntemann N, Sanner C, Lipphardt B, Tamm C and Peik E 2016 *Phys. Rev. Lett.* **116** 063001

[5] Aeppli A, Kim K, Warfield W, Safronova M S and Ye J 2024 *Phys. Rev. Lett.* **133** 023401

[6] Dimarcq N, Gertsvolf M, Mileti G, Bize S, Oates C, Peik E, Calonico D, Ido T, Tavella P, Meynadier F, *et al*. 2024 *Metrologia* **61** 012001

[7] Mehlstäubler T E, Grosche G, Lisdat C, Schmidt P O and Denker H 2018 *Reports on Progress in Physics* **81** 064401

[8] Lisdat C, Grosche G, Quintin N, Shi C, Raupach S, Grebing C, Nicolodi D, Stefani F, Al-Masoudi A, Dörscher S, *et al*. 2016 *Nat. Commun.* **7** 12443

[9] Exertier P, Samain E, Bonnefond P and Guillemot P 2010 *Advances in Space Research* **46** 1559

[10] Exertier P, Samain E, Martin N, Courde C, Laas-Bourez M, Foussard C and Guillemot P 2014 *Advances in Space Research* **54** 2371

[11] Giorgetta F R, Swann W C, Sinclair L C, Baumann E, Coddington I and Newbury N R 2013 *Nat. Photonics* **7** 434

[12] Shen Q, Guan J Y, Ren J G, Zeng T, Hou L, Li M, Cao Y, Han J J, Lian M Z, Chen Y W, *et al*. 2022 *Nature* **610** 661

[13] Caldwell E D, Sinclair L C, Newbury N R and Deschenes J D 2022 *Nature* **610** 667

[14] Caldwell E D, Deschenes J D, Ellis J, Swann W C, Stuhl B K, Bergeron H, Newbury N R and Sinclair L C 2023 *Nature* **618** 721

[15] Kong L, Cui K, Shi J, Zhu M and Li S 2022 *Journal of Lightwave Technology* **40** 252

[16] Itoh K 1982 *Applied Optics* **21** 2470

[17] Shen Q, Guan J Y, Zeng T, Lu Q M, Huang L, Cao Y, Chen J P, Tao T Q, Wu J C, Hou L, *et al*. 2021 *Optica* **8** 471

[18] Walsh M, Guay P and Genest J 2023 *APL Photonics* **8** 071302

[19] Oelker E, Hutson R, Kennedy C, Sonderhouse L, Bothwell T, Goban A, Kedar D, Sanner C, Robinson J, Marti G, *et al*. 2019 *Nat. Photonics* **13** 714

[20] Schioppo M, Brown R C, McGrew W F, Hinkley N, Fasano R J, Beloy K, Yoon T, Milani G, Nicolodi D, Sherman J, *et al*. 2017 *Nat. Photonics* **11** 48

[21] Ellis J L, Bodine M I, Swann W C, Stevenson S A, Caldwell E D, Sinclair L C, Newbury N R and Deschênes J D 2021 *Phys. Rev. Applied* **15** 034002

[22] Richards M A, *et al.* 2005 *Fundamentals of radar signal processing* Vol. 1 (New York: Mcgraw-Hill)